

Article

# Structural, Mechanical and Tribological Properties of NbCN-Ag Nanocomposite Films Deposited by Reactive Magnetron Sputtering

Fanjing Wu, Lihua Yu \*, Hongbo Ju, Isaac Asempah and Junhua Xu

School of Materials Science and Engineering, Jiangsu University of Science and Technology, Mengxi Road 2#, Zhenjiang 212003, China; fanjingwu6@163.com (F.W.); hbju@rocketmail.com (H.J.); nanasempah@yahoo.com (I.A.); jhxu@just.edu.cn (J.X.)

\* Correspondence: lhyu6@just.edu.cn; Tel.: +86-150-5111-9966; Fax: +86-511-8440-1184

Received: 13 December 2017; Accepted: 21 January 2018; Published: 29 January 2018

**Abstract:** In this study, reactive magnetron sputtering was applied for preparing NbCN-Ag films with different Ag additions. Ag contents in the as-deposited NbCN-Ag films were achieved by adjusting Ag target power. The composition, microstructure, mechanical properties, and tribological properties were characterized using energy-dispersive X-ray spectroscopy (EDS), X-ray diffraction (XRD), field emission scanning electron microscope (FE-SEM), high resolution transmission electron microscopy (HRTEM), Raman spectrometry, nano-indentation, and high-temperature sliding wear tests. Results indicated that face-centered cubic (fcc) NbN, hexagonal close-packed (hcp) NbN and fcc Ag, amorphous C and amorphous CN<sub>x</sub> phase co-existed in the as-deposited NbCN-Ag films. After doping with 2.0 at.% Ag, the hardness and elastic modulus reached a maximum value of 33 GPa and 340 GPa, respectively. Tribological properties were enhanced by adding Ag in NbCN-Ag films at room temperature. When the test temperature rose from 300 to 500 °C, the addition of Ag was found beneficial for the friction properties, showing a lowest friction coefficient of ~0.35 for NbCN-12.9 at.% Ag films at 500 °C. This was mainly attributed to the existence of AgO<sub>x</sub>, NbO<sub>x</sub>, and AgNbO<sub>x</sub> lubrication phases that acted as solid lubricants to modify the wear mechanism.

**Keywords:** NbCN-Ag films; magnetron sputtering; microstructure; tribological properties

## 1. Introduction

Transition metal nitrides (TMN), owing to a good combination of mechanical and physical properties, have potential for diverse applications ranging from electronic and optoelectronic devices to aerospace structures. Similarly, NbN based films also have been widely used in the field of microelectronics [1,2]. Due to their high hardness, good toughness, and excellent corrosion resistance, NbN based films are most suitable for using as functional films, especially on the surface of mould and on cutting tools for surface modifications. However, these films have a high friction coefficient during application [3]. Therefore, their poor resistance to plastic shearing and dry sliding wear have limited their applications.

In the past, in order to improve the low temperature lubrication performance of TMN based films, an effective method was to form graphite by doping carbon elements. For example, TiCN films were prepared by Cheng et al. [4], which outperformed TiN in tribological applications associated with carbon incorporation [5]. In addition, CrCN coating produced by the cathodic arc evaporation (CAE) deposition method showed higher hardness and tribological properties than CrN coatings [6].

Recently, soft metals (such as silver, aluminum, and copper) were added into TMN based films to reduce the friction coefficient over a wide temperature range [7–9]. As expected, a novel self-lubricated CrN-Ag nanocomposite film was elucidated by Mulligan et al. [10], indicating that the addition of

Ag improved the friction and wear properties of CrN films at 500 °C. Moreover, Ju et al. [9] studied the tribological properties of NbN/Ag films and the results showed that the migration of Ag and the formation of the silver niobium oxide ( $\text{AgNbO}_3$ ) with layer-by-layer assembly of amorphous structure at high temperature were the main reasons for the reduction of friction coefficients of NbN/Ag films. In previous study [11], a series of NbCN films with different C were deposited onto a Si substrate using the reactive magnetron sputtering method. However, with the increase of the sliding temperature, the friction coefficients were still relatively high. This is the fact that a single lubricant could not meet the requirements of excellent tribological properties over a wide temperature range. A series of TiCN-Ag [12], ZrCN-Ag [13], and MoCN-Ag [14] films were systematically prepared and the properties were also improved by adding Ag. Metallic silver, tungsten trioxide, and silver tungsten oxide phases coexisted in the magnetron sputtered WCN-Ag film produced by Xu et al. [15], as a result of the lower friction coefficient over a wide heating temperature range due to the existence of Ag phases.

Herein the NbCN-Ag films with different Ag content were deposited using the reactive magnetron sputtering technique. This paper aimed at disclosing the beneficial effects of Ag nanoparticles and lubrication phase ( $\text{AgO}_x$ ,  $\text{NbO}_x$ , and  $\text{AgNbO}_x$ ) on the modification of the microstructure and on the mechanical properties, as well as acting as solid lubricants to enhance wear resistance.

## 2. Experimental Details

### 2.1. Preparation of Films

NbCN-Ag composite films with a thickness of about 2  $\mu\text{m}$  were deposited on 304 stainless steel and Si (100) wafers using the JGP-450 series single chamber magnetron sputtering system. Si (100) wafers were used as substrate materials for structural and mechanical investigations. Stainless steel 304 was used as substrate material for the dry sliding ball-on-disk tests. The Nb, Ag, and C targets each had a diameter and purity of 75 mm and 99.9% respectively and were sputtered with three radio frequency powers. The target-substrate distance was 78 mm with no substrate bias voltage. Before being placed on the substrate holder in the chamber, the substrates were cleaned with successive rinses in ultrasonic baths of acetone and alcohol and blown dry with dry air. Ar (99.999%) and  $\text{N}_2$  (99.999%) were introduced into the chamber by two gas inlets after the chamber was pumped to a pressure of  $6 \times 10^{-4}$  Pa.

Using magnetron sputtering using a voltage of 220 V, NbCN-Ag films with various Ag content were obtained by fixing the power of the Nb and C targets at 200 W (current: 0.91 A) and 120 W (current: 0.55 A) respectively and adjusting the power of the Ag target from 0 W (current: 0 A), 20 W (current: 0.09 A), 30 W (current: 0.14 A), 40 W (current: 0.18 A), and 50 W (current: 0.23 A) while maintaining a constant working pressure (0.3 Pa) with an Ar and  $\text{N}_2$  flow rate of 10:5 sccm in a radio-frequency magnetron sputtering system. All the samples were labeled corresponding to the content of Ag (e.g., NbCN-2.0 at.% Ag, NbCN-12.9 at.% Ag etc.)

### 2.2. Characterization of the Films

The phases of NbCN-Ag films were explored by X-ray diffraction (XRD, Shimadzu-6000, Shimadzu, Kyoto, Japan) with a Cu  $K\alpha$  source, operating at 40 kV and 35 mA. The scanning speed was 4°/min. The average grain crystal size ( $D_c$ ) of NbN was calculated by the Debye-Scherrer equation [16]:

$$D_c = \frac{0.89\lambda}{B \cdot \cos\theta} \quad (1)$$

where  $\lambda$  is the X-ray wavelength,  $B$  is the full width at half maximum (FWHM) of the diffraction peak, and  $\theta$  represents the diffraction angle. The diffraction profiles were corrected for the instrumental broadening using an alumina sample, which had large crystallites free from defects. The cross-sections of the films were observed by field emission scanning electron microscopy (FE-SEM, Merlin Compact-6170, ZEISS, Jena, Germany). A high-resolution transmission electron microscopy (HRTEM, JEM-2010F, JEOL, Tokyo, Japan) operated at an accelerating voltage of 200 kV and energy

dispersive spectroscopy (EDS) on an EDAX DX-4 energy dispersive analyzer were used to characterize the crystallinity, microstructure and elemental composition of the film. The hardness and elastic modulus of the films were determined by a nano-indenter CPX + NHT<sup>2</sup> + MST equipped with a diamond Berkovich indenter tip (3-sided pyramid). In order to minimize the substrate's influence on the hardness of the films, a maximum load of 3 mN was used to meet the  $d/h < 0.1$  criterion (where  $d$  and  $h$  are the indenter penetration depth into the film and the film thickness, respectively). Nine points were selected for each sample and averaged. An automatic indentation mode was programmed to place indentations in a  $3 \times 3$  array. Each sample was tested three times. Fused silica was used as a reference sample for the calibration before indents were made.

The tribological properties of specimens were conducted along a circular track with a diameter of 8 mm against an Al<sub>2</sub>O<sub>3</sub> counterpart having a diameter of 9 mm for a period of 30 min. A constant speed of 50 rpm was maintained with a normal load of 3 N in an atmosphere with a relative humidity of about 25–30% and a temperature range of 25 to 500 °C using a UTM-2 CETR tribometer. Friction tests were performed three times under the same conditions for the same batch of samples, and the accuracy of the experiment was confirmed based on the repeatability of the experimental results. Thereafter, a profilometer (Bruker DEKTAK-XT, Billerica, MA, USA) was used to determine wear volume loss of the films ( $V$ ) by examining the worn tracks. Each sample was repeated three times. In order to calculate the wear rates ( $W$ ) of the as-deposited films, an Archard's classical wear equation [17] was listed as follows:

$$W = \frac{V}{S \times L} \quad (2)$$

where,  $S$  represents the sliding distance,  $L$  is the loading force, and  $V$  is wear volume. After wear tests, the wear tracks were also detected by XRD (Shimadzu-600). We fixed the spot on the wear tracks, the spot size was 1.0 mm, and the wear tracks were larger than the spot size.

A micro-Raman spectrometer (inVia\*, Renishaw, Gloucestershire, UK) having a 514.5 nm Ar<sup>+</sup> laser as an excitation source with back scattering geometry was used in recording Raman spectra at room temperature. In addition, films on AISI 304 stainless steel substrates were used for dry sliding wear measurements. For the reproducibility of experimental results, the above mechanical tests were repeated three times under the same conditions.

### 3. Results and Discussion

#### 3.1. Composition and Phase Structure for NbCN-Ag Films

Chemical composition of the as-deposited NbCN-Ag films was determined by energy dispersive spectroscopy, as depicted in Figure 1. The content of N was nearly constant at ~32 at.%. C content was slightly reduced from 31 to 29.1 at.%. With an increase of Ag target power extending from 0 to 50 W, there was an opposite variation expression for the amount of Nb and Ag in the NbCN-Ag films. In contrast, Nb content decreased from 36.8 at.% to 25.7 at.% relative to that of Ag content which increased from 0 to 12.9 at.%. According to the regulation of Ag target power ranging from 0 to 50 W, various Ag contents were detected. Ag content in the as-deposited NbCN-Ag films was adjusted through Ag target power. The accuracy of the carbon and nitrogen content was limited by the EDS method.

XRD patterns obtained for films with different Ag contents are shown in Figure 2. Pure NbN film displayed four diffraction peaks centered at  $35.4^\circ$ ,  $39.0^\circ$ ,  $41.1^\circ$ ,  $59.5^\circ$  which were assigned to the face-centered cubic (fcc) NbN (111) (JCPDF 38-1155), hexagonal close-packed (hcp) NbN (101) (JCPDF 14-0547), fcc-NbN (200) (220) (JCPDF 38-1155) respectively. As shown in Figure 2, without Ag addition, the measured value was approximately  $34.8^\circ$ ,  $38.0^\circ$ ,  $40.5^\circ$ , and  $58.7^\circ$  which is smaller than standard value. Compared with NbN, the peak shift is a result of lattice distortion caused by incorporation of C into NbN to form NbCN. Many researches on NbN-based thin films have shown that high nitrogen flow rate and sputtering bias voltage were the main reasons for their formation [18,19]. With the Ag content increased further, the diffraction peak is gradually shifted to a large angle, which due to the Ag

particles present on the boundaries of NbN phases could squeeze the grain to cause lattice distortion. The lattice spacing of NbN then decreases. The decrease of the lattice constant of the NbN phases could result in the shift of the peak to a larger angle. Interestingly, with an increase of Ag content to 12.9 at.%, the sample exhibited two reflections at  $44.47^\circ$  and  $64.78^\circ$  corresponding to typical fcc-Ag (200) and fcc-Ag (220) peaks. Therefore, this suggests that when the Ag content reaches a certain amount, fcc-NbN, hcp-NbN, and Ag crystals co-exist in the NbCN-Ag films.

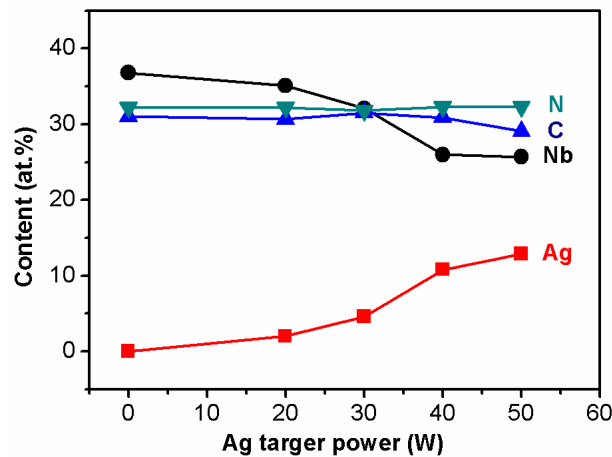


Figure 1. The chemical compositions of NbCN-Ag composite films.

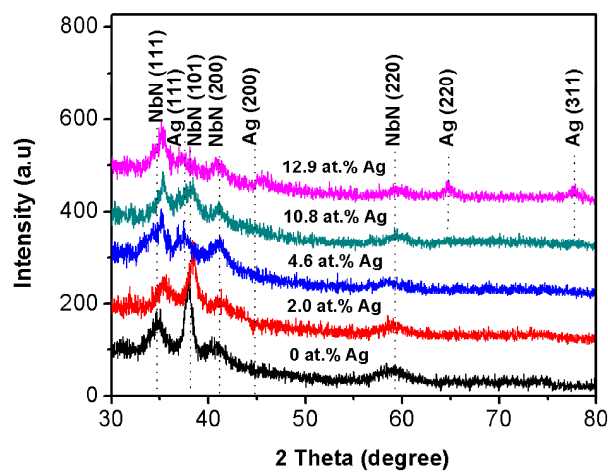


Figure 2. X-ray diffraction (XRD) patterns of NbCN-Ag composite films with different Ag content.

According to the determination from the above XRD patterns, it was found that the XRD diffraction intensity of NbN (101) decreased with the increase of Ag content. Based on Equation (1), the classical Debye-Scherer equation, the average grain sizes were calculated according to the values of  $\lambda$  and  $B$  listed in Table 1. Three measurements were made for each value. The results are shown in Figure 3, the grain size of NbN decreased gradually with increasing Ag content, thereby achieving a minimal refined grain texture of 15.50 nm at 12.9 at.% Ag.

**Table 1.** The values of  $\lambda$  and B obtained from XRD patterns.

Ag Content (at.%)	$\lambda$ (nm)	$B_{\text{NbN}(101)}$ ( $^{\circ}$ )
0		$0.462 \pm 0.002$
2.0		$0.504 \pm 0.003$
4.6	0.154	$0.515 \pm 0.002$
10.8		$0.534 \pm 0.001$
12.9		$0.673 \pm 0.002$

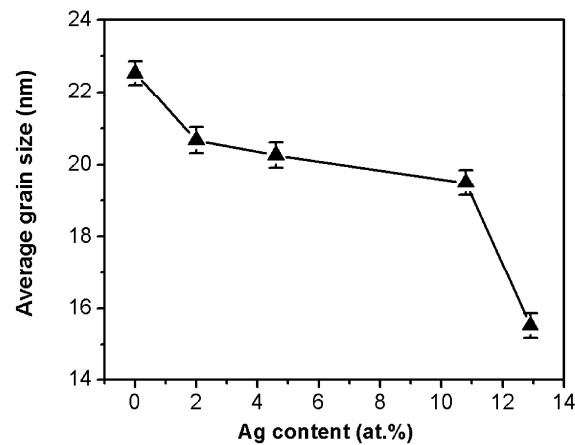
**Figure 3.** Grain sizes of NbCN phase with different content of Ag.

Figure 4 displayed the back scattered electron (BSE) images and SEM observations of NbCN-Ag composite film with different contents of Ag. Figure 4a,b are BSE images of NbCN-Ag films at 2.0 at.% Ag to distinguish between Ag and the crystalline substrate. BSE-EDS line scanning of the small particles is carried out in Figure 4a, which indicates that the white particles (arrows) in the BSE diagram are dispersed Ag particles. Figure 4c,d are SEM images of NbCN with various Ag content (4.6 at.% and 12.9 at.%) in order to observe the distribution of particles. From Figure 4, it can be seen that the dispersion of Ag particles increased with increasing Ag content in the as-deposited NbCN-Ag composite films. This result illustrated that the distribution of Ag particles was associated with the value of Ag target power. It is speculated that the effect of grain refinement was the result of the specific locations of the nano-scale Ag particles on the surface of NbN embryos that acted as heterogeneous nucleation sites to simulate finer crystallites.

In order to further confirm the state in which Ag existed in the NbCN-Ag films, the microstructure of NbCN-Ag composite films was revealed by the cross-sectional HRTEM images, as shown in Figure 5. As shown in Figure 5a, NbCN-Ag films had a columnar crystal. The inset in Figure 5a is the selected area electron diffraction (SAED) pattern of the film, showing fcc-Ag (220), fcc-NbN (111), (200), and hcp-NbN (101) diffraction rings. Two sets of lattice fringes with lattice spacing of about 0.259 nm and 0.236 nm (standard value: fcc-NbN (111) = 0.254 nm, hcp-NbN (101) = 0.231 nm) were observed, which were indicative of fcc-NbN (111) and hcp-NbN (101) (Figure 5b). The Ag particles present on the boundaries of the NbN phases could squeeze the grain to cause lattice distortion. This is in agreement with the results obtained from the corresponding XRD pattern (Figure 2). This indicates that fcc-NbN, h-NbN and fcc-Ag coexist. HRTEM was carried out in Figure 5c. A lattice fringe with lattice spacing of about 0.259 nm was detected, which was indicative of fcc-NbN (111).

TEM and HRTEM of NbCN-12.9 at.% Ag films are shown in Figure 5d–f. As drawn in Figure 5d, a columnar crystal texture was found for the NbCN-Ag film, also showing that the added Ag particles were well dispersed in the film. These results were consistent with the study of NbN-Ag composite films by Ju et al. [9]. From Figure 5e, two sets of lattice fringes with lattice spacing of about 0.236 nm and 0.259 nm were observed, which interrelated with hcp-NbN (101) and fcc-NbN (111). As determined

from the inserted SAED pattern in Figure 5e, three distinct diffraction rings corresponding to hcp-NbN (101), fcc-NbN (111), and fcc-Ag (220) were found, indicating Ag still existed in the form of elementary Ag metal. HRTEM, Fast Fourier Transform (FFT), and Inverse Fast Fourier Transform (IFFT) were carried out. The HRTEM, FFT, and IFFT images of the selected area are marked in Figure 5f, FFT filtering representing the structure of face-centered cube, lattice fringes with lattice spacing of 0.199 nm was detected and this value was almost the same as the calculated XRD value for fcc-Ag (200). Based on the XRD, SEM, and HRTEM analysis, within the range of measured Ag content, the films consisted of fcc-NbN, h-NbN, and Ag phase. In addition, the content of Ag phase increased with the increasing power of the Ag target. In Figure 2, when the Ag content was lower than 12.9 at.%, the Ag phase was not detected, which is due to the low content of Ag phase.

In addition, the formation of amorphous phase also reduced the grain size. In order to obtain further information about the carbon containing phase, the Raman spectra obtained from three different Ag contents of NbCN-Ag films are shown in Figure 6. Several authors have assigned the carbon phase, such as D bands at  $1351\text{ cm}^{-1}$  and G bands at  $1574\text{ cm}^{-1}$ , as well as C–N and C=N at  $1550\text{ cm}^{-1}$  and  $1750\text{ cm}^{-1}$  [13,20]. The symbols of D and G bands, typical for amorphous carbon and graphitic materials, started to appear with an increase in silver, which confirmed the presence of amorphous phase in the films. Compared with NbN, amorphous carbon phases are more easily formed under the same conditions due to the low Gibbs free energy. However, during the deposition process, the phase formation is also related to many other conditions, such as  $\text{N}_2$  concentration, temperature, and reaction atoms. After adding Ag target, some Ag atoms would cause sputtering of the deposited Nb away from the substrate to reduce Nb. In addition, Ag presents on the boundaries of NbN. This could provide the growth conditions for amorphous phases.

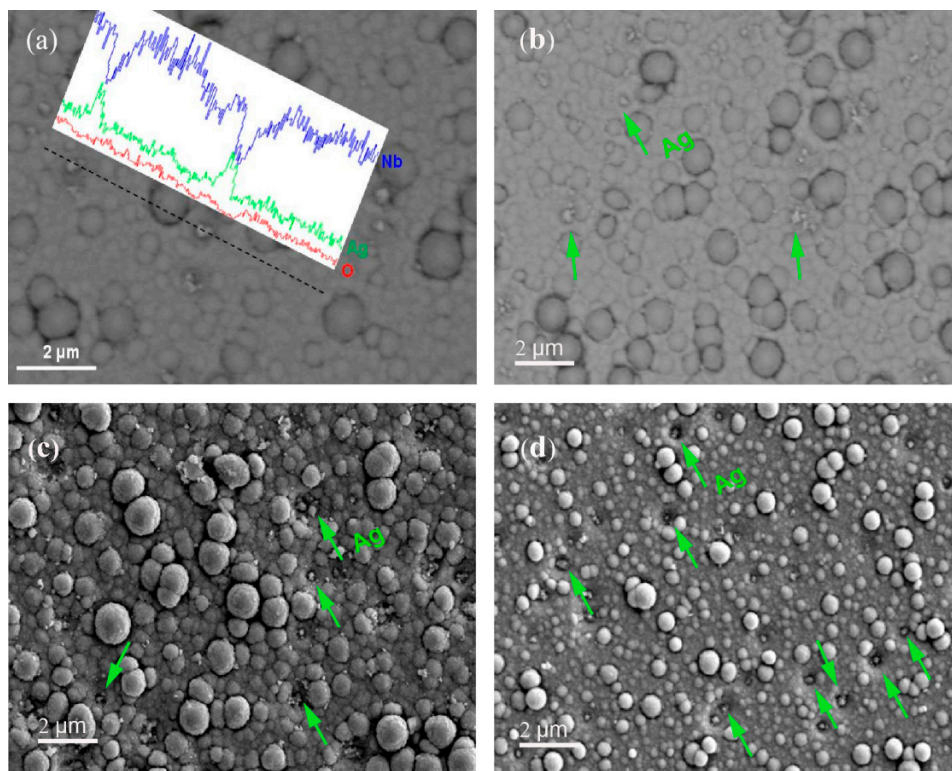


**Figure 4.** Back scattered electron images (a,b) and scanning electron microscopy (SEM) observations (c,d) of NbCN-Ag composite films with various Ag content: (a) line scan at 2.0 at.% Ag; (b) 2.0 at.% Ag; (c) 4.6 at.% Ag; (d) 12.9 at.% Ag.

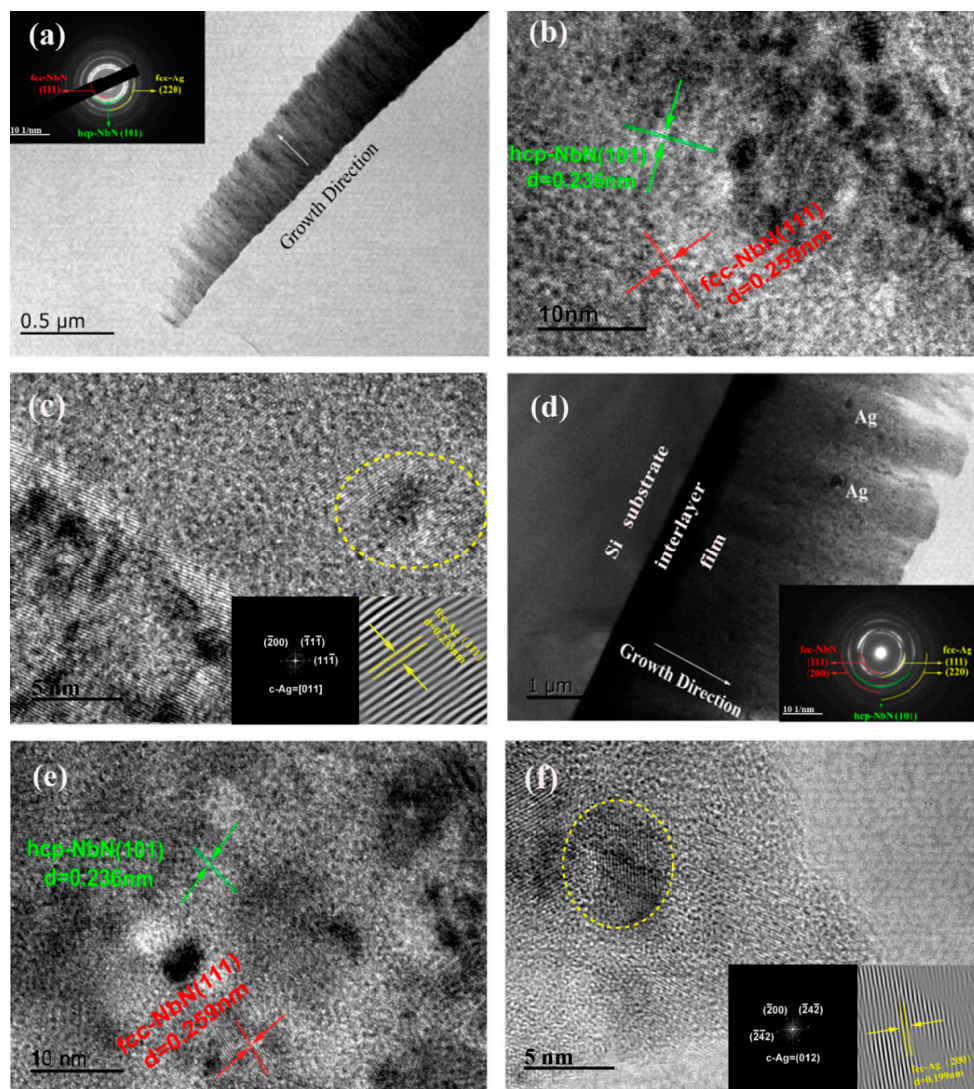


**Figure 5.** Transmission electron microscopy (TEM) and high resolution (HR)-TEM observations of NbCN-2.0 at.% Ag (a–c) and NbCN-12.9 at.% Ag (d–f) films. Inserts are the selected area electron diffraction (SAED) patterns for located areas.

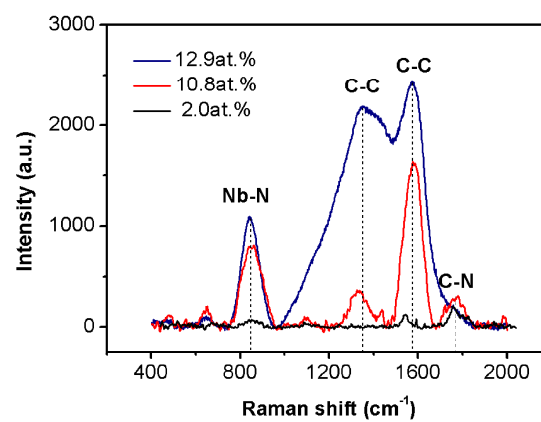


**Figure 6.** Raman spectrum of NbCN-Ag composite films at 2.0 at.%, 4.6 at.%, and 12.9 at.% Ag.

The characteristic value of Raman shift located at  $843\text{ cm}^{-1}$  was indicative of the vibrational frequencies of NbN [21]. Also its strength increased with an increase in Ag content, which was due to the surface enhanced Raman scattering effect of Ag. When the Ag molecule was adsorbed on the surface of the films, the Raman signal intensity was higher than the expected value by simple calculation [22]. With an increase in Ag content, the Raman signal enhancement rate of NbN was improved, and the intensity of the NbN peak increased with the increase of Ag content.

The decrease in Nb content with higher Ag content in the films suggested that, the formation of an additional amorphous graphite and amorphous  $\text{CN}_x$  amorphous phase increased. Therefore, it could be implied that the coarsening growth of the grains in the film was inhibited by the presence of the amorphous phases, which also led to the finer-grained size of NbCN-Ag films [15,20].

Based on the above analysis, it suggests that NbCN-Ag film consists of fcc-NbN, h-NbN, Ag phase, and amorphous C and  $\text{CN}_x$  phase. In addition, the content of amorphous C,  $\text{CN}_x$ , and Ag phase increased with the increase of Ag content.

### 3.2. Mechanical Properties

The micro-hardness ( $H$ ) and elastic modulus ( $E_r$ ) of NbCN-Ag composite films with different Ag content are shown in Figure 7. The estimated values of  $H$  and  $E_r$  for ternary NbCN film were about 30 GPa and 336 GPa, respectively.

As the Ag content increased from 0 to 2.0 at.%, the hardness and the elastic modulus increased slightly. When the content of Ag increased from 2.0 to 12.9 at.%, the hardness and elastic modulus decreased rapidly. With the addition of 2.0 at.% Ag, the value of  $H$  and  $E_r$  for NbCN-Ag films reached a maximum value of 33 GPa and 340 GPa.

When the content of Ag was relatively low, the hardness of NbCN-Ag composite films was mainly attributed to the effect of fine grain strengthening (Figure 4). Since the Ag content is relatively small, the corresponding increase in hardness was also small. When the content of Ag was high, the soft silver phase increased. At this point, the decrease of hardness due to the incorporation of silver weakens the effect of grain strengthening. In addition, with an increase in Ag content, the content of amorphous C (2 GPa [23]) and  $\text{CN}_x$  (4 GPa [24]) increased, resulting in a sharp decline in the hardness of films.

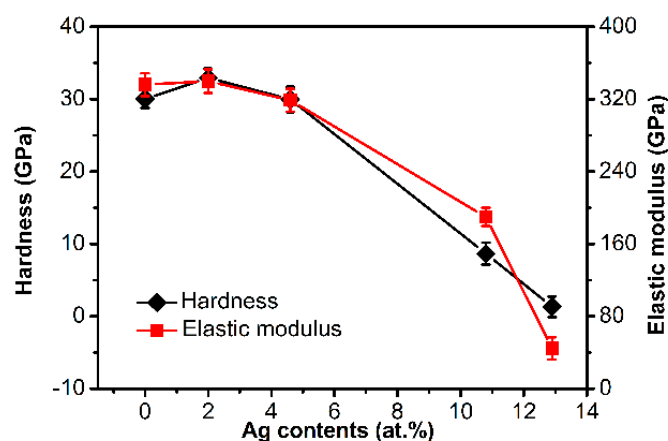


Figure 7. Micro-hardness and elastic modulus of NbCN-Ag composite films with different Ag contents.

### 3.3. Tribological Properties

#### 3.3.1. Tribological Properties at Room Temperature

Figure 8 shows the average friction coefficients and wear rates of NbCN-Ag films with different Ag contents. As shown, the average friction coefficient and wear rates of NbCN film were  $\sim 0.36$  and  $0.77 \times 10^{-7} \text{ mm}^3 \cdot \text{N}^{-1} \cdot \text{m}^{-1}$ . When the content of Ag increased to 2.0 at.%, the friction coefficients

of NbCN-Ag composite films drastically increased, and the wear rate decreased until it attained a minimum of  $0.15 \times 10^{-7} \text{ mm}^3 \cdot \text{N}^{-1} \cdot \text{m}^{-1}$ . As the content of Ag increased from 2.0 to 12.9 at%, the friction coefficients decreased rapidly and reached a minimum value of 0.28, while the wear rates of NbCN-Ag films increased.

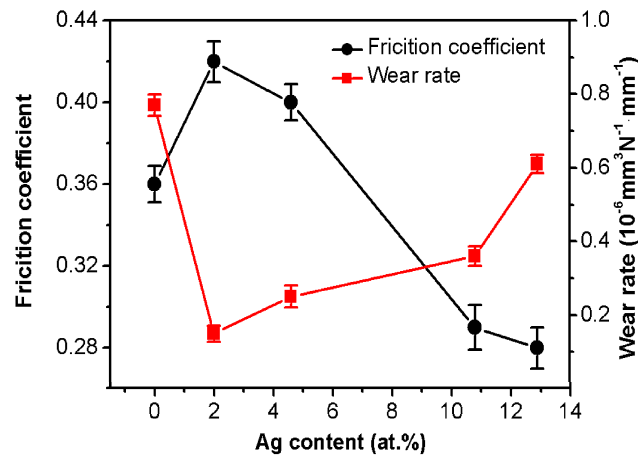


**Figure 8.** Friction coefficients and wear rates of NbCN-Ag composite films with different Ag contents.

According to the structural analysis, the content of soft Ag, amorphous C, and  $\text{CN}_x$  increased with increasing Ag content, which acted as a solid lubricant phase to reduce the friction coefficients of the films.

Wear theory indicates that [25,26] hardness is the main factor that affects the wear resistance of the material surface. The wear resistance of the material is also closely related to its structure. Graphite has a layered structure, and although it can reduce the average friction coefficient of the film, it is easily worn. When the content of Ag increased to 2.0 at.%, the hardness of the film increased (Figure 7), and the graphite content was relatively low (Figure 6), resulting in a decrease in wear rate. When the content of Ag was higher than 2.0 at.%, the hardness of the composite films were reduced, and the content of graphite with poor wear resistance increased, resulting in an increase of wear rate. In the dry friction experiment, when contact stress was applied, the hard coating could resist the elastic deformation caused by abrasive wear and low elastic modulus [9]. Therefore,  $H/E_r$  can be regarded as a key factor affecting the wear rate, while the resistance to the plastic deformation coefficient ( $H^3/E_r^2$ ) is also related to the wear rate. The  $H/E_r$  and  $H^3/E_r^2$  ratio of NbCN-Ag films with various Ag contents are shown in Figure 9, the ratios of  $H/E_r$  and  $H^3/E_r^2$  of NbCN film were 0.09 and 0.24, respectively. The  $H/E_r$  and  $H^3/E_r^2$  ratios of NbCN-Ag films, initially increased gradually and reached a maximum value, then decreased with increasing Ag content in the films, the maximum values were 0.097 and 0.31 at 2.0 at.% Ag, respectively. The wear rates of NbCN-Ag films, all of which were lower than that of NbCN film, were due to the low shear strength of the existing Ag that co-existed in the NbCN matrix [27]. Therefore, it was easier to shear under a loading force and the lower tangential force resulted in a lower plow stress, thus reducing the wear resistance.

Figure 10 shows SEM images of worn tracks for NbCN-2.0 at.% Ag films and NbCN-12.9 at.% Ag films after sliding for 30 min. The worn surface of the films is smooth without obvious peeling. The wear scar of NbCN-Ag film with Ag content of 2.0 at.% is narrow (Figure 10a), whereas the film with Ag content of 12.9 at.% is deep and rough (Figure 10b).

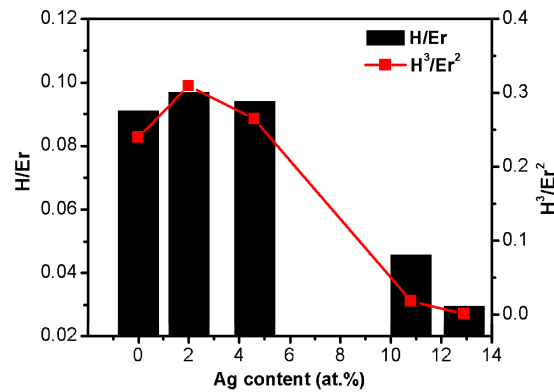


**Figure 9.** The ratios of  $H/E$  and  $H^3/E_r^2$  for NbCN-Ag composite films with different Ag contents.

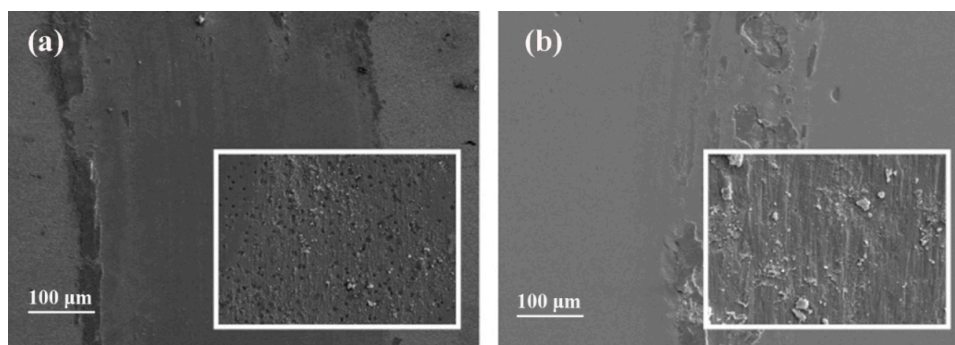


**Figure 10.** SEM image of worn track of NbCN-Ag composite films with different Ag contents: (a) 2.0 at.%; (b) 12.9 at.%.

### 3.3.2. Tribological Properties at Elevated Temperature

In order to study the tribological properties at elevated temperature, the friction coefficients and wear rates of NbCN and NbCN-12.9 at.% Ag films at different temperatures are presented in Figure 11. From room temperature (25 °C) to 300 °C, the friction coefficients of NbCN and NbCN-Ag films increased. Further increase to 500 °C, presented an opposite trend. The wear rates of NbCN and the NbCN-12.9 at.% Ag films increased slowly and was then followed by rapid growth. Moreover, the friction coefficients of NbCN-12.9 at.% Ag films were lower than that of NbCN film under the same testing condition. As soon as the testing temperature exceeded 200 °C, the wear rates of NbCN-12.9 at.% Ag films were higher than that of NbCN films, and reached a maximum value of  $6.7 \times 10^{-7} \text{ mm}^3 \cdot \text{N}^{-1} \cdot \text{m}^{-1}$  at 500 °C.

XRD patterns for worn products of NbCN-12.9 at.% Ag film after sliding at different temperatures are plotted in Figure 12. The diffraction peaks of  $\text{Nb}_2\text{O}_5$  increased with increasing temperature. This suggested that NbCN was oxidized to  $\text{Nb}_2\text{O}_5$ . When it reached 500 °C,  $\text{AgNbO}_3$  and  $\text{Ag}_2\text{O}$  were detected. The increasing peak intensities suggested that the oxidation became more severe with increase of the testing temperature.

To better study the oxide phases, Raman spectroscopy was used to evaluate wear track of NbCN-12.9 at.% Ag film after sliding at 300 °C and 500 °C, and the Raman spectra are shown in Figure 13. For NbCN-12.9 at.% Ag films after sliding at 300 °C, the Raman spectrum curve (Figure 13a, curve 1) obtained from outside of the wear track consisted of three peaks at about  $698 \text{ cm}^{-1}$ ,  $820 \text{ cm}^{-1}$  and  $1564 \text{ cm}^{-1}$  corresponding to Nb-O, Nb-N, C-C peaks [15,20,24], the same peaks were observed from the Raman spectrum curve (Figure 13b, curve 2) obtained from the wear track. The presence of  $\text{Nb}_2\text{O}_5$  indicated that oxidation occurred at this temperature. In addition, the intensity of the  $\text{Nb}_2\text{O}_5$  peak in curve 2 was higher than that in curve 1, which indicated that more oxide  $\text{Nb}_2\text{O}_5$  was formed. This was consistent with the XRD results in Figure 12.

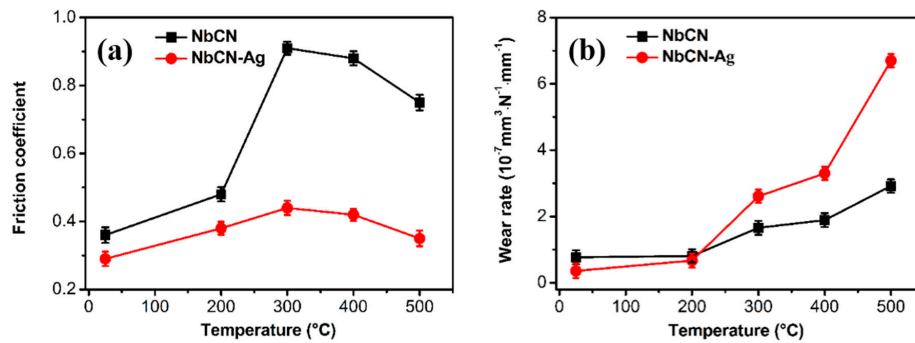


**Figure 11.** (a) Friction coefficients and (b) wear rates of NbCN and NbCN-12.9 at.% Ag film at different temperatures.

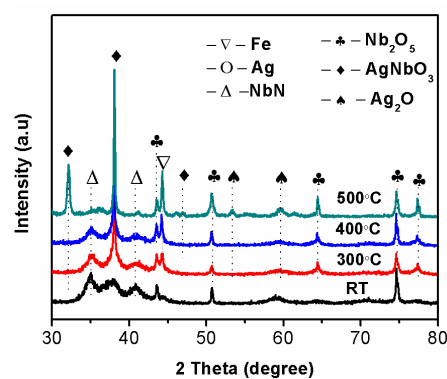


**Figure 12.** XRD patterns of NbCN-12.9 at.% Ag composite films after sliding at different temperatures.

For NbCN-12.9 at.% Ag films after sliding at 500 °C (Figure 13b), the Raman spectrum from outside the wear track was indicative of three peaks located at 698  $\text{cm}^{-1}$ , 820  $\text{cm}^{-1}$ , and 1564  $\text{cm}^{-1}$ , which are associated with  $\text{Nb}_2\text{O}_5$ , NbN and amorphous C, respectively. These three peaks which were similar to peaks from outside the wear track were detected. Furthermore, two strong peaks at 597  $\text{cm}^{-1}$  and 1294  $\text{cm}^{-1}$  were detected. They were delegated as the characteristic peaks of Ag-Nb-O and Ag-O vibration levels [9,13]. As discussed above, wear track contained  $\text{AgNbO}_3$  and  $\text{Ag}_2\text{O}$ , and the peak value only presented at the scratching place. Also, the intensity of the  $\text{Nb}_2\text{O}_5$  peak in curve 2 was higher than that in curve 1. Besides  $\text{Nb}_2\text{O}_5$ ,  $\text{AgNbO}_3$ , and  $\text{Ag}_2\text{O}$  were also formed. The results obtained from the Raman spectrum also confirm that the oxidation of the films becomes severe with an increase of the testing temperature.

With the temperature extending from RT to 300 °C, the friction coefficients of NbCN and NbCN-Ag composite films appeared to give an increasing trend. This was because, as the testing temperature increased, the water vapor in the environment disappeared, and C and  $\text{CN}_x$  in the lubrication phase generated  $\text{CO}_2$ , which led to the disappearance of lubrication medium [15]. As a result, the film surface adsorption disappeared and the friction coefficients increased under dry friction conditions. The increase in friction coefficient of NbCN-Ag films was obviously smaller than that of NbCN film. This was ascribed to the diffusion of Ag atoms under the action of heat, and the formation of a lubricating interface layer on the surface of the films. The results are in good agreement with the study by Mulligan et al. [28,29] with the high temperature friction reaction of CrN-Ag nanocomposite coatings. With an increase in temperature, the content of  $\text{Nb}_2\text{O}_5$  increased gradually, leading into a decrease in friction coefficient of NbCN film and NbCN-Ag composite films. It can also be observed that, the friction coefficients of NbCN-Ag composite films were much lower than that of NbCN film during testing at 300–500 °C, which was mainly due to the formation of an Ag lubricating layer with its oxides ( $\text{Ag}_2\text{O}$  and  $\text{AgNbO}_3$ ) on the film surface.

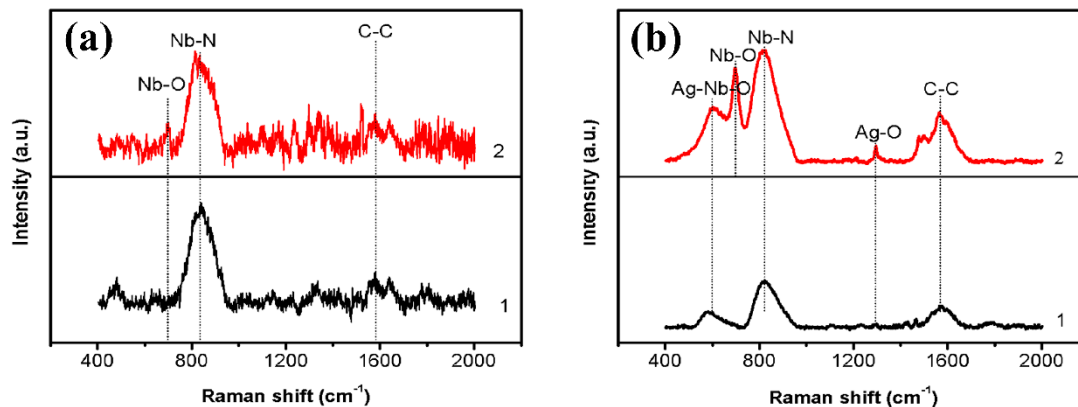


**Figure 13.** Raman spectra of worn tracks of NbCN-12.9 at.% Ag film at (a) 300 °C and (b) 500 °C.

SEM image of the wear track, 3D, 2D images, and EDS analysis of the NbCN-12.9 at.% Ag film at 300 and 500 °C were combined and are shown in Figure 14. Figure 14a,b shows the SEM surface of the wear surface at different temperatures. There are some debris (Figure 14a) and some plow and scratches (Figure 14b) on the surface of the scratches. For the wear marks for the 2D, 3D tests, (Figure 14c–f), when the temperature was 300 °C, the film wear surface was relatively smooth, with a small amount of furrow and a little bit of debris on the surface. When the temperature was 500 °C, the wear color became darker, the width became wider, and the oxidation was obvious. According to Figure 14g,h, the content of O and Ag increased. This suggested that the oxidation became serious and the diffusion of Ag to the surface increased with the increase of temperature.

The increase of the wear rates of NbCN film and NbCN-Ag films was mainly due to the following reasons:

- The oxidation of the films became serious due to the increasing in temperature. Nb<sub>2</sub>O<sub>5</sub> had a layered structure [10], which was highly diffusible and easily worn.
- The oxidation of C would also increase the wear rates at high temperature. When the temperature reached 300 °C, the wear rates of NbCN-Ag composite films were higher than that of NbCN film, which was due to the formation of a large amount of AgNbO<sub>3</sub> and Ag<sub>2</sub>O. This could aggravate the wear rates of the NbCN-Ag films.
- During the testing of friction, wear and deformation occurred on the Ag lubrication films. Due to the small surface strength of the films, the worn Ag chip had a tendency of dual disc adhesion, and the friction heating intensified the transfer of Ag [30]. The friction surface favored forming metal adhesion to aggravate the rate of wear, resulting in the severely deeper abrasive grooves on the worn tracks for NbCN film. (4) As the temperature increased from 300 °C to 500 °C, more Ag atoms diffused to the surface, which made the film hollow and easy to wear [14,31].

As the temperature increased from 300 to 500 °C, more Ag atoms diffused to the surface of the NbCN-Ag composite films, thereby characterizing some ploughs and scratches, as well as smooth and metallic adhesion without oxide residuals, piled up at the edge of scratch grooves. Obviously, the wear behavior was governed by a combination of plough friction, abrasive, and slight adhesive mechanisms. Thus worn surfaces of NbCN-12.9 at.% Ag composite films were typical of less scuffing, small ploughing, and some extent of slight abrasion, which was based on the pull out of soft Ag phase or its AgNbO<sub>3</sub> and Ag<sub>2</sub>O that emerged in the process of friction. For the existing shallower grooves, this was related to the abrasive Ag-rich worn products that were exposed from massive precipitations of Ag addition giving self-repairing effects on completed surface defective regions of the coatings [32].

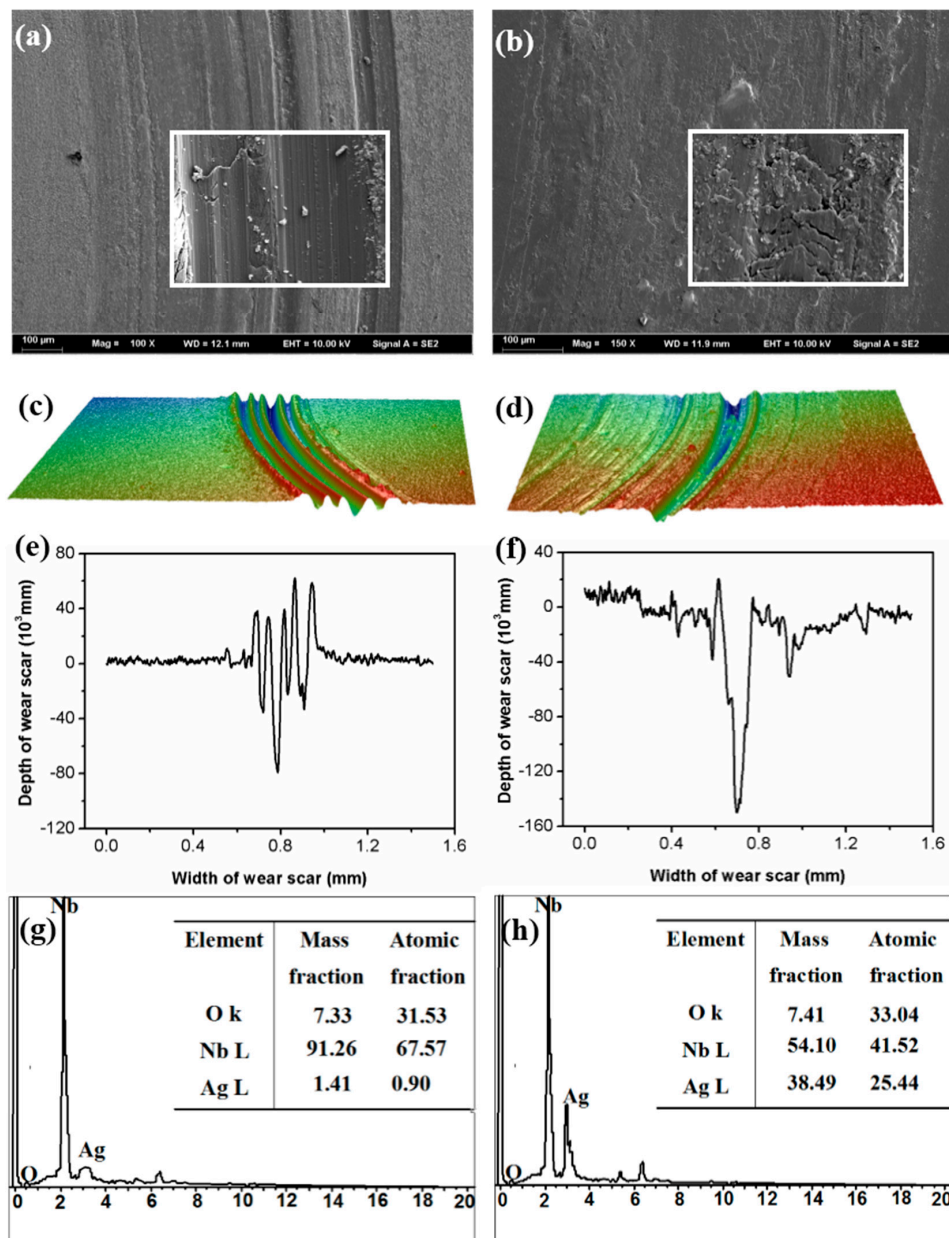


**Figure 14.** SEM (a,b) and three-dimension profiles of the worn surface (c,d), the corresponding cross-sectional profiles (e,f), and EDS analysis (g,h) of the selected ranges of NbCN-12.9 at.% Ag composite film at 300 °C and 500 °C.

#### 4. Conclusions

In summary, a novel NbCN-Ag film was successfully deposited onto 304 stainless steel and Si (100) substrate using the reactive magnetron sputtering method. According to analysis by XRD, Raman spectroscopy, and HR-TEM, the film consisted of a mixture of face-centered cubic fcc-NbN, hexagonal close-packed h-NbN, fcc-Ag phase, and amorphous C and CN<sub>x</sub> phase. Meanwhile, the content of amorphous C, CN<sub>x</sub>, and Ag phases increased with the increase of Ag content.

The estimated values of hardness and elastic modulus for the ternary NbCN film were about 30 GPa and 336 GPa, respectively. The hardness and elastic modulus of NbCN-Ag films first increased, followed by a rapid growth with increasing Ag content. As the content of Ag was 2.0 at.%, the hardness and elastic modulus of the films reached a maximum value of ~33 GPa and 340 GPa respectively. The average friction coefficient and wear rates of NbCN film were ~0.36 and  $0.77 \times 10^{-7} \text{ mm}^3 \cdot \text{N}^{-1} \cdot \text{m}^{-1}$ .

As the content of Ag was lower than 2.0 at.%, the friction coefficient of film increased gradually, and the wear rate decreased until it reached a minimum of  $0.15 \times 10^{-7} \text{ mm}^3 \cdot \text{N}^{-1} \cdot \text{m}^{-1}$ . When the content of Ag varied from 2.0 to 12.9 at.%, the friction coefficient decreased rapidly. When the temperature increased from 300 to 500 °C, the friction coefficient of NbCN-12.9 at.% Ag films significantly decreased and the wear rate showed an opposite trend. This was attributed to the generation of Nb<sub>2</sub>O<sub>5</sub>, AgNbO<sub>3</sub>, and Ag<sub>2</sub>O oxides that co-existed on the surface of worn tracks which acted as solid lubricants at elevated temperatures. However, these oxides share a lower shear strength and can be worn away under the sliding force. This results in an increase of the wear rate.

**Acknowledgments:** Special thanks for the financial support from the National Natural Science Foundation of China (Grant No. 51374115 and 51574131).

**Author Contributions:** Lihua Yu conceived and designed the experiments; Lihua Yu and Fanjing Wu performed the experiments and analyzed the data; Hongbo Ju, Isaac Asempah and Junhua Xu contributed to data analysis; Lihua Yu wrote the paper; all authors participated and discussed this work and contributed to the submitted and published manuscript.

**Conflicts of Interest:** The authors declare no conflict of interest.

## References

1. Ezirmik, K.V.; Rouhi, S. Influence of Cu additions on the mechanical and wear properties of NbN coatings. *Surf. Coat. Technol.* **2014**, *260*, 179–185. [[CrossRef](#)]
2. Cansever, N.; Danışman, M.; Kazmanlı, K. The effect of nitrogen pressure on cathodic arc deposited NbN thin films. *Surf. Coat. Technol.* **2008**, *202*, 5919–5923. [[CrossRef](#)]
3. Zhang, K.; Balasubramanian, K.; Ozsdolay, B.D.; Mulligan, C.P.; Khare, S.V.; Zheng, W.T.; Gall, D. Epitaxial NbC<sub>x</sub>N<sub>1-x</sub>(001) layers: Growth, mechanical properties, and electrical resistivity. *Surf. Coat. Technol.* **2015**, *277*, 136–143. [[CrossRef](#)]
4. Cheng, Y.H.; Browne, T.; Heckerman, B.; Meletis, E.I. Influence of the C content on the mechanical and tribological properties of the TiCN coatings deposited by LAFAD technique. *Surf. Coat. Technol.* **2011**, *205*, 4024–4029. [[CrossRef](#)]
5. Zhang, K.; Wen, M.; Wang, S.; Deng, R.P.; Gall, D.; Zheng, W.T. Sputter deposited NbC<sub>x</sub>N<sub>y</sub> films: Effect of nitrogen content on structure and mechanical and tribological properties. *Surf. Coat. Technol.* **2014**, *258*, 746–753. [[CrossRef](#)]
6. Tong, C.Y.; Lee, J.W.; Kuo, C.C.; Huang, S.H.; Chan, Y.C.; Chen, H.W.; Duh, J.G. Effects of carbon content on the microstructure and mechanical property of cathodic arc evaporation deposited CrCN thin films. *Surf. Coat. Technol.* **2013**, *231*, 482–486. [[CrossRef](#)]
7. Velasco, S.C.; Cavaleiro, A.; Carvalho, S. Functional properties of ceramic-Ag nanocomposite coatings produced by magnetron sputtering. *Prog. Mater. Sci.* **2016**, *84*, 158–191. [[CrossRef](#)]
8. Kelly, P.J.; Li, H.; Benson, P.S.; Whitehead, K.A.; Verran, J.; Arnell, R.D.; Iordanova, I. Comparison of the tribological and antimicrobial properties of CrN/Ag, ZrN/Ag, TiN/Ag, and TiN/Cu nanocomposite coatings. *Surf. Coat. Technol.* **2010**, *205*, 1606–1610. [[CrossRef](#)]
9. Ju, H.; Xu, J. Microstructure and tribological properties of NbN-Ag composite films by reactive magnetron sputtering. *Appl. Surf. Sci.* **2015**, *355*, 878–883. [[CrossRef](#)]
10. Mulligan, C.P.; Blanchet, T.A.; Gall, D. CrN-Ag nanocomposite coatings: Tribology at room temperature and during a temperature ramp. *Surf. Coat. Technol.* **2010**, *204*, 1388–1394. [[CrossRef](#)]
11. Kiryu, S.; Shoji, A.; Kohjiro, S.; Kodaira, S. Stress in NbC<sub>x</sub>N<sub>1-x</sub> films prepared by reactive RF magnetron sputtering. *Jpn. J. Appl. Phys.* **1993**, *32*, L834–L836. [[CrossRef](#)]
12. Sánchez-López, J.C.; Abad, M.D.; Carvalho, I.; Galindo, R.E.; Benito, N.; Ribeiro, S.; Henriques, M.; Cavaleiro, A.; Carvalho, S. Influence of silver content on the tribomechanical behavior on Ag-TiCN bioactive coatings. *Surf. Coat. Technol.* **2012**, *206*, 2192–2198. [[CrossRef](#)]
13. Ferreri, I.; Lopes, V.; Calderon, V.S. Study of the effect of the silver content on the structure and mechanical behavior of Ag-ZrCN coatings for orthopedic prostheses. *Mater. Sci. Eng. C* **2014**, *42*, 782–790. [[CrossRef](#)] [[PubMed](#)]

14. Shtansky, D.V.; Bondarev, A.V.; Kiryukhantsev-Korneev, P.V. Structure and tribological properties of MoCN-Ag coatings in the temperature range of 25–700 °C. *Appl. Surf. Sci.* **2013**, *273*, 408–414. [[CrossRef](#)]
15. Yu, L.; Zhao, H.; Xu, J. Influence of silver content on structure, mechanical and tribological properties of WCN-Ag films. *Mater. Charact.* **2016**, *114*, 136–145. [[CrossRef](#)]
16. Xu, J.; Chen, J.; Yu, L. Influence of Si content on the microstructure and mechanical properties of VSiN films deposited by reactive magnetron sputtering. *Vacuum* **2016**, *131*, 51–57. [[CrossRef](#)]
17. Shi, J.; Muders, C.M.; Kumar, A.; Jiang, X.; Pei, Z.L.; Gong, J.; Sun, C. Study on nanocomposite Ti-Al-Si-Cu-N films with various Si contents deposited by cathodic vacuum arc ion plating. *Appl. Surf. Sci.* **2012**, *258*, 9642–9649. [[CrossRef](#)]
18. Singh, K.; Bidaye, A.C.; Suri, A.K. Magnetron sputtered NbN films with electroplated Cr interlayer. *Vacuum* **2011**, *86*, 267–274. [[CrossRef](#)]
19. Wang, J.; Song, Z.; Xu, K. Influence of sputtering bias on the microstructure and properties of Nb-Si-N films. *Surf. Coat. Technol.* **2007**, *201*, 4931–4934. [[CrossRef](#)]
20. Carvalho, I.; Henriques, M.; Oliveira, J.C.; Alves, C.F.A.A.; Piedade, P.; Carvalho, S. Influence of surface features on the adhesion of Staphylococcus epidermidis to Ag-TiCN thin films. *Sci. Technol. Adv. Mater.* **2013**, *14*, 35009–35018. [[CrossRef](#)] [[PubMed](#)]
21. Kaiser, R.; Spengler, W.; Schicktanz, S.; Politis, C. Raman Spectra and Superconductivity of Various Phases of a High-Tc Superconductor: NbN. *Phys. Status Solidi* **1978**, *87*, 565–573. [[CrossRef](#)]
22. Stone, D.S.; Migas, J.; Martini, A. Adaptive NbN/Ag coatings for high temperature tribological applications. *Surf. Coat. Technol.* **2012**, *206*, 4316–4321. [[CrossRef](#)]
23. Prabhakaran, V.; Talke, F.E. Wear and hardness of carbon overcoats on magnetic recording sliders. *Wear* **2000**, *243*, 18–24. [[CrossRef](#)]
24. Qi, J.; Luo, J.; Wen, S. Structure, mechanical and tribological properties of carbon nitride thin films. *Vac. Sci. Technol.* **2000**, *6*, 381–384. (In Chinese)
25. Erdemir, A. A crystal-chemical approach to lubrication by solid oxides. *Tribol. Lett.* **2000**, *8*, 97–102. [[CrossRef](#)]
26. Jouve, G.; Severac, C.; Cantacuzene, S. XPS study of NbN and (Nb Ti)N superconducting coatings. *Thin Solid Films* **1996**, *28*, 146–153. [[CrossRef](#)]
27. Yu, K.Y.; Liu, Y.; Rios, S.; Wang, H.; Zhang, X. Strengthening mechanisms of Ag/Ni immiscible multilayers with fcc/fcc interface. *Surf. Coat. Technol.* **2013**, *237*, 269–275. [[CrossRef](#)]
28. Waterhouse, G.I.N.; Bowmaker, G.A.; Metson, J.B. The thermal decomposition of silver (I, III) oxide: A combined XRD, FT-IR and Raman spectroscopic study. *Phys. Chem. Chem. Phys.* **2001**, *3*, 3838–3845. [[CrossRef](#)]
29. Mulligana, C.P.; Blanchetb, T.A.; Galla, D. CrN-Ag nanocomposite coatings: High-temperature tribological response. *Wear* **2010**, *269*, 125–131. [[CrossRef](#)]
30. Erdemir, A. A crystal chemical approach to the formulation of self-lubricating composite coatings. *Surf. Coat. Technol.* **2005**, *200*, 1792–1796. [[CrossRef](#)]
31. Bondarev, A.V.; Kiryukhantsev-Korneev, P.V.; Sidorenko, D.A.; Shtansky, D.V. A new insight into hard low friction MoCN-Ag coatings intended for applications in wide temperature range. *Mater. Des.* **2015**, *93*, 63–72. [[CrossRef](#)]
32. Ju, H.; Xu, J.; Yu, L. Effects of Mo content on the microstructure and friction and wear properties of TiMoN films. *Acta Metall. Sin.* **2012**, *48*, 1132–1138.

